AIAA SciTech Forum
11–15 & 19–21 January 2021, VIRTUAL EVENT
AIAA Scitech 2021 Forum

10.2514/6.2021-0334

Experimental Investigation of Atmospheric Induced Beam Jitter

Matthew Kalensky[*a], Eric J. Jumper[†a], Stanislav Gordeyev[‡a],
Matthew Kemnetz[b], Aaron Archibald[c]

[a]*University of Notre Dame, Notre Dame, Indiana, 46556*
[b]*Air Force Research Laboratory, Kirtland AFB, NM, 87117*
[c]*Air Force Institute of Technology, Wright-Patterson AFB, OH, 45433*

AAOL-BC was employed to conduct experiments which sought to measure atmospheric induced jitter on a laser beam. Wavefronts were collected for a laser beam which was propagated between two aircraft at varying altitudes and separations. A data processing procedure for extracting the turbulence induced jitter is presented and the resulting jitter and higher order wavefront aberrations were used to extract turbulence parameters such as C_n^2 and r_0. The resulting turbulence quantities using these various approaches are compared with literature. It was shown that data collected at lower altitudes and large aircraft separations resulted in up to 5 μrad of tilt onto the laser beam. Using the measured atmospheric induced jitter, C_n^2 values were extracted which lined up well with models prevalent in literature, such as HV57. Values of C_n^2 which were approximated using higher order wavefront statistics were generally higher than what is predicted by turbulence models due to contamination from the aero-optical and aero-acoustical environments around the aircraft.

Nomenclature

C_n^2	= Index of refraction structure constant
D	= Aperture diameter
D_ϕ	= Phase structure function
f	= Frequency
κ	= Wavenumber
L	= Range
λ	= Wavelength
U	= Velocity
$\vec{r}$	= Two-dimensional position vector
r_0	= Atmospheric coherence length
Φ	= Energy spectrum
ϕ	= Phase
σ_x	= Streamwise rms jitter
σ_{HO}^2	= Phase variance

I. Introduction

tudying the propagation of lasers through the atmosphere is important for the development of aircraft mounted high Senergy laser (HEL) technology, optical communications, imaging, and astronomical sensing [1]. The statistically

[*] Graduate Researcher, AIAA student member, mkalensk@nd.edu
[†] Professor, Department of Aerospace and Mechanical Eng., AIAA Fellow
[‡] Associate Professor, Department of Aerospace and Mechanical Eng., AIAA Fellow

random fluctuations of refractive index in the atmospheric medium are deleterious to the functionality and operation of these systems [1]. The use of airborne directed energy laser weapon systems offers great promise for next generation defense applications. Fully realized and operational airborne HELs necessitate research into fundamental physics on laser propagation through different turbulence environments. The term jitter, as it is used here, is defined as the angular pointing error of the beam sourced from primarily mechanical disturbances and vibrations of optical elements in the beam director. One of the functions of a beam control system is to track and maintain an aim point on the target. Therefore, it is desirable for system designers to mitigate beam jitter. Other researchers (see Ref. [2], for example) have recognized that motion through the turbulent atmosphere also imposes jitter on the laser beam. In this work, jitter imposed onto the laser beam by the atmosphere will be experimentally investigated using the Airborne Aero-Optics Laboratory for Beam Control (AAOL-BC). Atmospheric induced jitter as well as higher order laser distortions will also be used to extract optical turbulence parameters such as C_n^2 and r_0. These results will be compared with literature.

Section II introduces common atmospheric turbulence parameters as well as key differences between atmospheric turbulence and aero-optical turbulence environments. Section III discusses the experimental campaign objectives, setups, and test parameters. Section IV describes the necessary data processing procedure for handling these wavefront data. Section V presents results for the measured atmospheric induced jitter at various test points. Section VI compares three approaches for using the measured wavefronts to extract turbulence parameters and the advantages and disadvantages of each approach are discussed.

II. Background

A. Atmospheric Optical Turbulence

Due to the random nature of the atmosphere as well as its dependence on many independent variables, predicting instantaneous characteristics of the turbulent atmosphere is difficult. Therefore, Kolmorogov suggested a theory that was statistically motivated and is centered around the idea of an energy cascade, where energy is injected at the largest scales and cascades down to smaller scales via turbulent eddy interactions until eventually the remaining energy is dissipated as heat [3, 4, 5]. In the intermediate region, referred to as the inertial subrange, the energy at each scale is a function of structure size only. Obukhov built on the work of Kolmorogov and showed that in the atmosphere, temperature can be modeled as a conservative passive scalar and therefore, using a similar procedure as Kolmogorov, arrived at an energy spectrum for temperature [6, 7]. Much of the atmospherics community today still refers to the text of Tatarskii as he applied his predecessor's theoretical constructs to wave propagation in turbulence [8]. By relating temperature fluctuations to index of refraction fluctuations, Tatarskii outlined how the index of refraction structure constant, C_n^2, is an elegant way to describe both the scale size of the index of refraction fluctuations as well as the magnitude of the resultant aberrations [7]. For this reason, this parameter is of utmost value to the laser propagation through atmospheric turbulence community. Using the findings established by Kolmogorov, Obukov, and Tatarskii, additional useful turbulence parameters have since been derived. One of these parameters is the atmospheric coherence length or parameter, r_0. Otherwise known as the Fried parameter, r_0 is qualitatively defined as the aperture size that can be used which will result in 1 rad of wavefront phase error [9]. For environments of constant C_n^2, the atmospheric coherence length for plane waves is described by Eq. 1. For spherical waves and constant C_n^2 along the propagation path, the Fried coherence length can be described by Eq. 2 . Here, L is the propagation range and κ is the wavenumber defined as $2\pi/\lambda$, where λ is the laser wavelength [9, 10].

$$r_0 = 1.68(C_n^2 L\kappa^2)^{-3/5} \tag{1}$$

$$r_0 = 3.0(C_n^2 L\kappa^2)^{-\frac{3}{5}} \tag{2}$$

B. Atmospheric v. Aero-Optical Environments

Very different discussions revolve around the aero-optics community versus the atmospheric propagation community. Both research thrusts are imperative to understand for the successful development of an airborne HEL system. So why

do these different disciplines, both centered around the idea of laser propagation through turbulence, warrant such different research treatments? Fundamentally, a major difference between the two types of environments is the size of the aberrating turbulent structures. In the atmosphere, index of refraction changes are resultant from large turbulent structures (outer scales), which are typically much larger than the laser system's aperture. These structures are caused by atmospheric wind shear and variations of temperature within the atmosphere [7]. As mentioned, temperature is treated as a passive scalar so the theory described above which makes use of structure functions, can be applied. The use of the index of refraction structure constant, C_n^2, is a concise way to quantify the intensity of the optical turbulence environment, but the ability to rely on C_n^2 depends on the atmospheric optical turbulence being "Kolmogorov" [7]. For a turbulence environment to be "Kolmogorov," the assumptions of homogeneity and isotropy must apply. Additionally, to calculate the structure function necessary to quantify this parameter, the viewing aperture must be within the inertial range. The definition of the phase structure function, D_ϕ, can be seen in Eq. 3, where ϕ is the phase and $\vec{r}$ is the separation between measurement locations. Additionally, the relationship between this phase structure function and the atmospheric coherence length, r_0 can be found in Eq. 4 [9, 10].

$$D_\phi(\vec{r}) = \langle[\phi(r_1 + \vec{r}) - \phi(r_1)]^2\rangle \tag{3}$$

$$D_\phi(\vec{r}) = 6.88\left(\frac{\vec{r}}{r_0}\right)^{5/3} \tag{4}$$

For the case of aero-optical turbulence, the turbulence is produced at length scales on the order of the aperture size and generally, aerodynamic flows are not typically homogeneous or isotropic. Aero-optical induced distortions are resultant from either compressibility effects when speeds exceed Mach 0.3 or local unsteady pressure fluctuations associated with aerodynamic flow environments such as boundary layers or separated shear layers [11]. In addition, at high transonic and supersonic speeds, unsteady shocks will be an additional source of aero-optical distortions. The work here seeks to isolate the beam distortion contribution from the atmosphere. However, the beam will propagate through both the atmosphere as well as the aero-optical boundary layer of the aircraft. Therefore, it is important to understand how these two aberrating environments are coupled.

C. Extracting Turbulence Parameters from Wavefront Data

An ability to extract optical turbulence characteristics from wavefront measurements is useful for system designers. For these experiments, the wavefronts of a laser beam which has propagated through the atmosphere at various altitudes and path lengths are collected. As described above, three different approaches are used to extract turbulence parameters, C_n^2 and r_0, from the wavefronts. Each of these approaches are described in the sections to come. Many researchers have extensively investigated recovering optical turbulence parameters from wavefront measurements. In this work, atmospheric optical turbulence parameters are extracted from environments which are also subjected to aero-optical, aero-acoustical, and atmospheric distortions to the wavefronts. Therefore, the ability of each approach to quantify atmospheric optical turbulence will depend on how the effects of the atmosphere are dissociated from the effects of the aerodynamic flow.

1. Single Axis Jitter Variance

Ultimately, the experimental campaigns described in this work are conducted to quantify atmospheric induced jitter. The acquisition aperture acts as a spatial filter, where optical turbulence structures larger than the aperture manifest as tip/tilt and optical turbulence structures smaller than the aperture manifest as higher order distortions. There are two definitions of tip/tilt prevalent in the literature: G-tilt and Z-tilt. G-tilt is the result of averaging all local gradients over a wavefront. Z-tilt comes from the terms with radial degree one of the Zernike polynomial expansion. In this

work, the Z-tilt definition is used due to its physical relationship with jitter. Jitter is a far-field consequence of tip/tilt being imposed onto a laser's wavefront. In the absence of tip/tilt imposed by mechanical corruption, it is expected that the largest contribution of tip/tilt imposed onto the wavefronts comes from the atmosphere compared to the aero-optical and aero-acoustical environments around an aircraft. Therefore, using the global tip/tilt to extract optical turbulence quantities is a viable option. Equation 5 describes a relationship between the measured streamwise temporal root mean square (rms) tilt, σ_x, the atmospheric coherence length, r_0, the aperture size, D, and the wavelength of the laser used, λ [2, 10]. Since the jitter rms is measured experimentally and the aperture size as well as the wavelength are known system parameters, Eq. 5 can be solved for r_0. The calculated value for r_0 can then be used in Eq. 1 in order to approximate a C_n^2.

$$\sigma_x^2 = 0.182 \left(\frac{\lambda}{D}\right)^2 \left(\frac{D}{r_0}\right)^{5/3} \tag{5}$$

2. Tilt Removed Phase Variance

For these experiments, wavefronts of the laser beam which has propagated through the atmosphere, the turbulent boundary layer (TBL) of the aircraft, and the acoustical environment around the aircraft are measured. Equation 6 describes an analytical relationship between the tilt removed phase variance, σ_{HO}^2, and the atmospheric coherence length, r_0 [12], where D is the aperture diameter. After solving for r_0, Eq. 1 can be used to approximate a C_n^2. Previous researchers have showed that using the phase variance requires much more averaging in order to achieve a small estimation error for r_0 [13]. This method is also expected to be subjected to high error due to the aero-optical/acoustical environments as well as the inherently high averaging needed for statistical confidence. It was selected to be used here in order to highlight the utility of the single axis jitter rms approach for approximating optical turbulence characteristics.

$$\sigma_{HO}^2 = 1.34 \left(\frac{D}{r_0}\right)^{5/3} \tag{6}$$

3. Phase Structure Function

Lastly, the phase structure function will be used in order to extract turbulence quantities from the measured wavefronts. Here, the structure function can be calculated from experimental wavefront data using Eq. 3, this value can then be plugged into Eq. 4 to solve for r_0. The r_0 value can again be used with Eq. 1 to extract a C_n^2.

III. Experimental Setup

A. The Airborne Aero-Optics Laboratory for Beam Control (AAOL-BC)

The goal of the work is to measure, quantify, and characterize airborne measurements of atmospheric induced jitter. To do this, a laser beam is projected through the atmosphere at both varying altitudes as well as propagation distances using AAOL-BC. The primary objective of AAOL-BC is to provide an in-flight testing platform where aero-optics experiments can be performed under real conditions [14]. AAOL-BC consists of two Falcon-10 aircraft capable of flying at varying separations, altitudes, and Mach numbers. One aircraft, designated as the source aircraft, projects a 532 nm diverging laser beam onto a custom-designed optical quality window mounted on the second aircraft, referred to here as the laboratory aircraft. The window is mounted on a specially designed aluminum mount, meant to limit distortions to the attached boundary layer as fluid convects from the aircraft fuselage over the window [14]. The window has a clear aperture of 0.3048 m in diameter, with optical quality of better than $\lambda/10$ in surface flatness. For this experiment, the two AAOL-BC aircraft will fly at large separations to measure the jitter imposed by the atmosphere onto the laser beam. Presumably, large separations between aircraft as well as lower altitude flights will impose more atmospheric contribution. Since both aircraft are flying at the same altitude when each data point is collected, for the purposes of this work, it will be assumed that C_n^2 is nominally constant across the propagation path. Details pertaining to the systems installed on both AAOL-BC aircraft as well as the campaign test parameters will be discussed in greater detail in the next sections.

1. *AAOL-BC: Source Aircraft*

The source aircraft is equipped with a Laser Quantum Opus 532 *nm* 0-2 variable watt laser, motorized system to vary beam divergence, a 50 *mm* diameter OIM102 fast steering mirror (FSM), an AeroTech gimbal with a 100 *mm* mirror, a National Instruments PXI Real-Time system, a laptop for user control, and a GPS unit which allows relative aircraft displacements to be calculated. This system allows for both image and return based tracking capability. Figure 1 illustrates the experimental setup in the source aircraft. A wide field of view (WFOV) camera with a 300 *mm* lens was used to locate the laboratory aircraft and the narrow field of view (NFOV) camera with a 600 *mm* lens was used for tracking – either off the return signal or image features of the other aircraft. Using the motorized beam divergence system, the divergence of the outgoing beam can be changed by the user to sufficiently fill the acquisition window on the laboratory aircraft window regardless of the separation distance between aircraft.

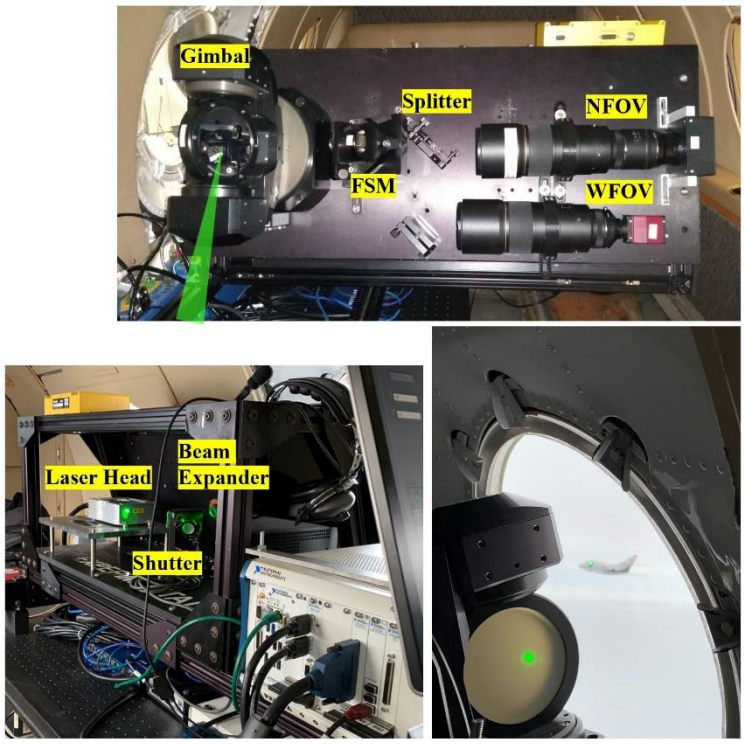

Figure 1. AAOL-BC source aircraft setup.

2. *AAOL-BC: Laboratory Aircraft*

The laboratory aircraft receives the incoming beam from the source aircraft and directs the beam to a Shack Hartmann Wavefront Sensor (SHWFS) installed on a high-speed camera. Figure 2 illustrates the experimental setup of this aircraft. Here, the beam enters through the optical quality window then is directed off a 304.8 *mm* flat steering mirror mounted on an AeroTech gimbal. To stabilize the incoming beam, a computer-controlled proportional feedback system was employed. The gimbal forwards the beam through a Schmidt-Cassegrain telescope with a diameter of 203 *mm* and a central obscuration of 64 *mm* in diameter. A mirror is mounted on the back of the telescope's secondary mirror in order to pick off a portion of the beam for the tracking camera which has a 500 *mm* focal length lens attached. After exiting the telescope, a portion of the beam is directed to an imaging camera and the other portion of the beam is split again to be partitioned between an On-Trak PSM2-10 position sensing device (PSD) as well as the SHWFS. The PSD sends velocity commands to the gimbal and serves as the fine track system. The SHWFS has a spatial resolution of 50x50 subapertures 0.3 *mm* in size, allowing the wavefront distortions imposed on the beam to be

measured with great spatial resolution. Wavefronts were acquired at both 4 and 10 kHz. A corner cube was also installed at the bottom of the aircraft acquisition window, ensuring that the source aircraft received a strong return signal for tracking at large separations.

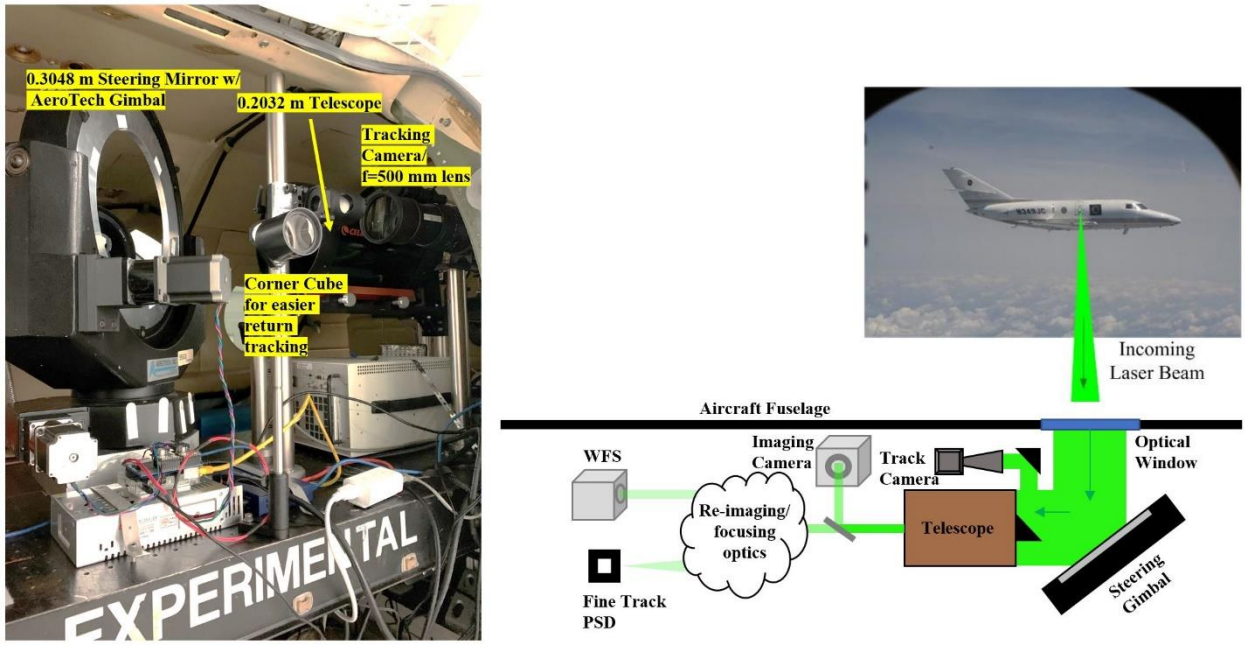

Figure 2. AAOL-BC laboratory aircraft setup.

3. Campaign Objectives

Wavefronts are collected at both varying altitudes and separations. The details pertaining to the data points collected in the two flights can be seen in Table 1. Flight 1 was conducted in the afternoon on 07 March 2020 and flight 2 was conducted in the late morning to early afternoon on 17 March 2020. Both flights were conducted over the Northern Michigan area. Wavefronts were collected at both 4 and 10 kHz with an exposure time of both 0.4 and 1 μs. The aircraft consistently flew at a cruise Mach number of 0.4 corresponding to a spatial overlap between consecutive wavefronts of approximately 83.5 % and 93.4 %, respectively for the two sample rates used. A total of 28,000 frames were collected per data point.

Table 1. Data matrix indicating altitudes and aircraft separations where wavefronts were collected.

Approximate Altitude [m]	Approximate Separation [m]					
	750	1500	2300	3000	3300	3700
762		X				
914		X				
1219		X				
1372	X	X				
1524	XO	XO	X	X	X	X
1829	X	X	XO	X	X	X
2134			O			
3048	O	O	O	O		

O: Flight 1; X: Flight 2; Shaded Blue: Data collected over water

IV. Processing Procedure

Since the measured wavefronts are susceptible to different contamination sources, various data processing procedures need to be applied to isolate the jitter quantities of interest. The atmosphere is comprised of a wide range of spatial scales of turbulent structures and the aperture is comparatively small. Therefore, it is expected that the largest contribution of aberrations onto the laser beam will be in the form of tip and tilt. Additionally, since the boundary layer of the aircraft is sufficiently smaller (δ ~40 mm) [14] than the size of the viewing aperture (D=0.2032 m), it will be assumed that minimal tip/tilt contribution comes from the TBL of the aircraft [15]. Therefore, the presumption is that most of the turbulence induced beam jitter comes from the atmospheric distortions. The TBL distortions will be in the form of higher order aberrations. Unfortunately, mechanical contamination introduces a corrupting source of jitter that is coupled with the atmospheric induced component of interest. A novel approach referred to as the "stitching method" has been developed which addresses a process for dissociating the mechanical contamination from the turbulence induced jitter that is desirable to quantify [16]. Additionally, it has been shown that acoustic contamination in the form of upstream propagating sound waves from the downstream located jet engine also introduce appreciable distortions onto the laser beam [14, 17]. The next few sections will outline the overall data reduction procedure and how to handle these sources of contamination.

A. Tip/Tilt/Piston and Steady Lensing Removal

Since the measured tip/tilt data is known to be corrupted with mechanical contamination, all tip/tilt is initially removed from the wavefront data. As mentioned above, when calculating and removing tip/tilt, there are two definitions prevalent in literature: gradient tilt (G-tilt) and Zernike tilt (Z-tilt). G-tilt is the result of averaging all local gradients over a wavefront. Z-tilt comes from the terms with radial degree one of the Zernike polynomial expansion. The Zernike series is comprised of sums of power series with scaling that imposes the orthogonality over a unit disk. Tip, tilt, and piston represent the three lowest order Zernike modes. In order to calculate Z-tilt, a least squares fit of a plane is applied to the wavefront. The error associated with the least squares fit of the wavefront plane is minimized by solving a system of linear equations and the resultant coefficients $A(t)$, $B(t)$, and $C(t)$, are the tip, tilt, and piston values, respectively [15,16]. The equation for error can be seen in Eq. 7. Here, the tip, tilt coefficients as a function of time are the "global" tilt. For the experimentally measured wavefronts, tip/tilt is extracted using this Z-tilt definition of jitter due to its physical connection to far-field jitter.

$$Error(A,B,C) = \iint_{Aperture} (WF(x,y,t) - [A(t)x + B(t)y + C(t)])^2 dxdy \tag{7}$$

Experimental data sets are also subject to a temporally steady or, quasi steady wavefront component, referred to as steady lensing. It is also necessary to remove steady lensing from the data set. Steady lensing is often removed for experimental data processing because it is assumed that an adaptive optics system can compensate for this distortion in typical applications. Here, steady lensing is removed by time averaging the wavefront over a specified time interval and removing this from all instantaneous wavefronts within that window. For the purposes of this work, a steady lensing averaging window of 0.25 s was selected. This window size selection is deliberate as choosing a window which is large may not remove all steady content and choosing a window which is too small will affect the ability of the stitching method in reintroducing the correct turbulence induced tip and tilt.

B. Stitching

Once tip, tilt, piston, and steady lensing have been removed from the data set, the stitching method can be applied to reintroduce the tip and tilt caused by the atmosphere. Stitching relies on the convective nature of the laser beam's aberrating structures. Since the aircraft cruise speed is known and the wavefronts are collected at high sampling rates, an overlap between consecutive frames exists. Using this novel stitching approach, tip and tilt in these overlap regions for the consecutive frames can be calculated. This can be visualized in Fig. 3.

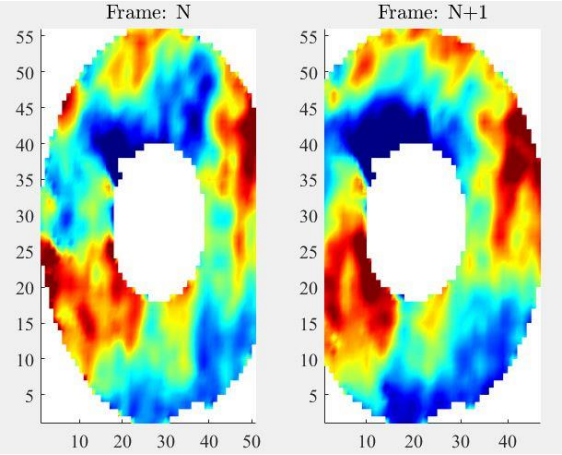

Figure 3. Overlap region of two consecutive wavefront frames.

Figure 3 shows the overlap region between two consecutive wavefront frames. It can be seen that many of the turbulent structures in the wavefront have slightly convected downstream from one frame to the next. The discrepancy in tip and tilt in this overlap region represents the tip and tilt contribution from turbulence that should not have been removed. Much greater detail on the stitching method can be found in Ref. [16]. In order to validate that the stitching method is working correctly, wave optics simulations were utilized. Here, a beam is propagated through a simulated atmosphere using Monte Carlo phase screens of a prescribed turbulence intensity, C_n^2. Greater detail describing the approach of generating these wave optics simulations can be found in Refs. [18,19,20]. Since there is no mechanical contamination present in these simulation results, stitching can be used to demonstrate that the tip, tilt, and piston which is initially removed can be correctly reintroduced. This validation is presented in Fig. 4. Here, the tilt time series which is initially removed from the simulated wavefronts is represented by the solid

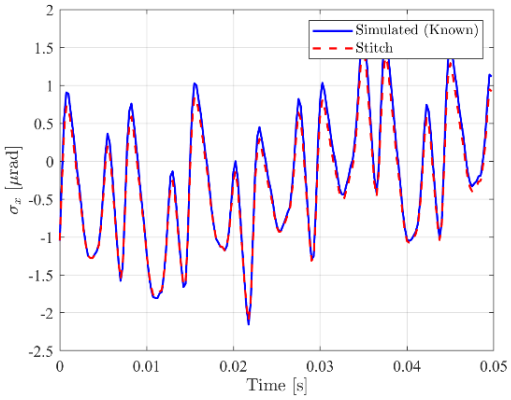

Figure 4. Comparison between simulated tilt time series and stitched tilt time series.

blue line. The tilt removed time series is then stitched. The dotted red line represents the tilt time series calculated using the stitching method. The two time series are in agreement – indicating the functionality of the stitching method.

C. Acoustic Contamination Removal

Another source of wavefront contamination comes from acoustic waves emanating from the jet engine located downstream of the optical quality acquisition window. These acoustic waves appear as upstream propagating spanwise uniform vertical structures with a frequency matching the blade pass frequency of the jet engine. Since these structures are upstream propagating (opposite the direction of convective turbulent structures), a three-dimensional fast Fourier transform, otherwise known as a dispersion analysis has been an effective means for isolating and removing this source of wavefront aberration [14,17]. Despite being an effective means for dissociating the upstream and downstream propagating disturbances for some applications, whether the new downstream time series will be successful in working with stitching to quantify atmospheric induced jitter is still not known. Using a circular aperture with a circular obscuration introduces non-physical spectral content and the influence of which on this research objective is still under investigation. However, perhaps removing the acoustic contamination is not necessary to begin with. If the stitching algorithm's robustness can handle the introduction of noise in the form of regular spanwise uniform upstream propagating structures, the dispersion analysis processing step can be avoided along with its associated challenges.

In order to test the idea presented above, where in certain instances, stitching may be tolerant to acoustic waves, we again resort to using wave optics simulations. Instead now, experimental data will be infused into the simulations in order to more accurately replicate the data measured in the long-range atmospheric jitter flight campaigns. Previous AAOL-BC campaigns consisted of the two Falcon 10 aircraft flying in close formation, rather than the long propagation ranges from the campaign emphasized in this work [11,14,17,21]. Since a laser beam propagated between aircraft which flew in close formation (nominally 50 m apart), the presumption is that there is negligible atmospheric induced effect - contrary to the studies that are being conducted now. These data were collected through only the naturally developing TBL on the AAOL-BC aircraft. For convenience, these previous studies will be referred to here as the "BL campaign", and it is expected that the laser beam is primarily distorted by the TBL and the acoustic waves. The BL campaign was also conducted at the same Mach number as the studies atmospheric studies emphasized in this work. Using these BL campaign flight data where the data acquisition environment closely mimics the current work, these data can be introduced into the atmospheric wave optics simulations to replicate the environment and data points seen in the current study. This work will shed light on the success of the stitching method in an environment where empirical TBL and acoustic data is introduced and the atmospheric effect is known (absent of mechanical contamination).

Since the simulated atmospheric wavefronts and the experimental wavefronts containing the boundary layer and acoustic information are slightly different spatial discretizations, the simulation wavefronts are interpolated onto a grid to match the experimental data. Additionally, the BL campaign data was sampled at 25 kHz, much faster than the atmospheric simulations. Therefore, to match the lower sampling rate, the BL campaign data is downsampled. The simulated and experimental wavefronts are then added together at each instant in time. This can be seen in Fig. 5 where the left image is a wavefront snapshot of the simulated atmosphere, the middle image is a wavefront snapshot of experimental data from the BL campaign, and the right most image is a combination of the left and middle images.

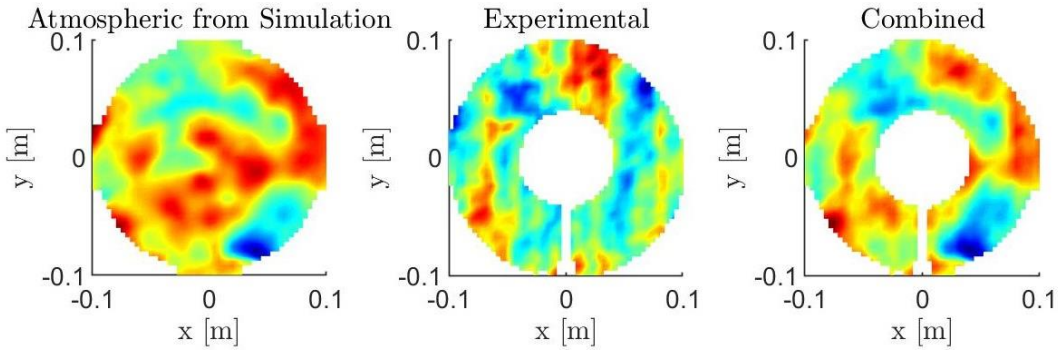

Figure 5. Comparison of a simulated wavefront frame of atmospheric propagation, experimental wavefront frame of data from the "BL campaign," and a wavefront frame of the two combined.

From here, the stitching procedure is applied to both the data set containing only the atmospheric simulation as well as the data set that is the combination of the atmospheric simulation with the experimental data. This allows a direct comparison to be made, indicating the error associated with leaving the acoustic effect in the data. The results of which can be seen in Fig. 6. Here the solid blue line represents the stitched jitter from just the atmospheric simulation and the dashed black line represents the stitched jitter from the atmospheric simulation combined with the experimental BL campaign data. The two jitter time series very closely match, indicating that leaving acoustic contamination in the data only mildly affects the success of the stitching method. Therefore, for processing the data emphasized in this work, the acoustic contamination is left in the data. The steps provided above, lay the groundwork for a new, application inspired data reduction procedure. The results to come will demonstrate the contribution of the atmosphere on laser beam distortions when projected to long range engagements.

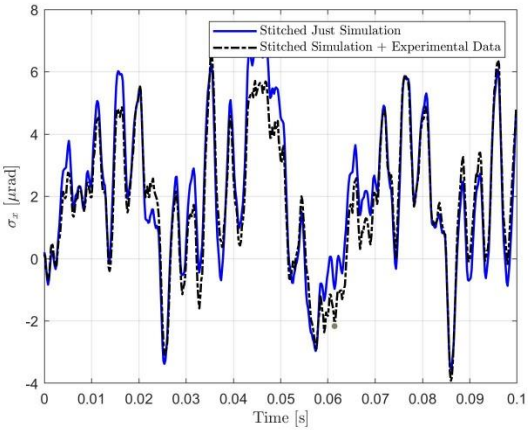

Figure 6. Stitching simulations containing atmospheric simulation and atmospheric simulations with experimental data added

V. Atmospheric Induced Jitter Results

Using the processing procedure described above, atmospheric induced jitter is extracted for various data points. Recall the aperture size on the AAOL-BC laboratory aircraft is *D=0.2 m* in diameter. The initial atmospheric induced jitter results for various aircraft separations and altitudes can be seen in Fig. 7. As expected, when the propagation distance is short (later referred to as short aircraft separation), there is only a small jitter contribution from the atmosphere. Additionally, the data points collected at higher altitudes were subjected to much less atmospheric induced jitter than the data points collected at low altitudes. This is also expected since the index of refraction structure constant, C_n^2, markedly drops with increasing altitude. For the data collected at an altitude of 3048 m, atmospheric induced jitter is only a weak function of propagation range. However, at an altitude of 1524 m, atmospheric induced jitter drastically increases to approximately 5 μrad for an aircraft separation of about 1.5 km. Previous work utilized wave optics simulations in order to computationally predict the jitter imposed on a beam after propagation through various C_n^2 environments between AAOL-BC aircraft. The experimental results presented in Fig. 7, are compared with these computational results in Fig. 8 [18]. The atmospheric induced jitter extracted from experimental data is in agreement with the computationally predicted jitter values from realistic C_n^2 environments. This figure provides insight as to what turbulence parameters may be expected based on calculated jitter. The next section will investigate how the measured atmospheric induced jitter as well as the wavefronts will be used to quantify the atmospheric turbulence environment in which the data was collected.

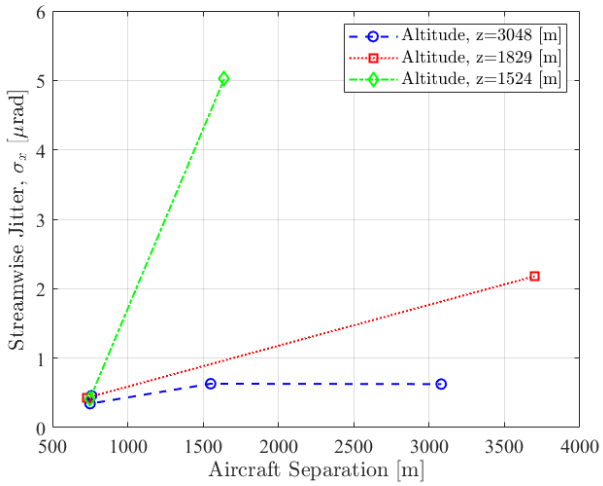

Figure 7. Extracted atmospheric induced jitter for data points collected at various altitudes and aircraft separations.

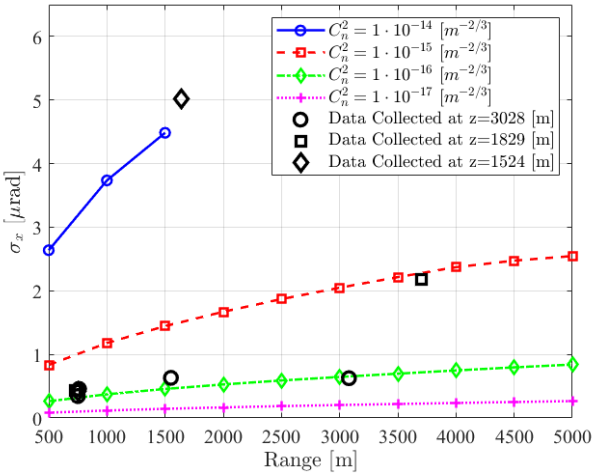

Figure 8. Experimentally measured atmospheric induced jitter compared with jitter computationally predicted using wave optics simulations.

VI. Extracting Turbulence Parameters

Section IIC presented three approaches which allow optical turbulence parameters r_0 and C_n^2 to be extracted from wavefront measurements. Each of these approaches is employed on the data points taken at various aircraft separations and altitudes. The atmospheric coherence length, r_0 is calculated for each data point using each of the approaches and is then used to find C_n^2. The results of which can be seen in Fig. 9. Here, it can be seen that the C_n^2 values calculated using the atmospheric induced jitter approach are lower than the C_n^2 values calculated using the tilt removed phase variance as well as the phase structure function approaches. This is expected since the tilt removed phase variance and phase structure function approaches utilize higher order wavefront content to make an r_0 estimate. In addition to the atmosphere, the TBL of the aircraft as well as the acoustic waves of the jet engine will impose higher order aberrations. Therefore, it is expected that the extracted r_0 is smaller compared to an r_0 calculated from only the atmosphere's higher order distortion contribution. The approach which makes use of the atmospheric induced jitter is not as influenced by the aero-optical and aero-acoustical environments around the aircraft since most of the turbulence induced tip/tilt comes from the atmosphere. Therefore, this approach produces the highest confidence results. The experimentally extracted C_n^2 values are also compared with altitude dependent turbulence models commonly seen in the literature; Hufnagel Valley 5-7 Model (HV57), Clear Night 1 Model, and SLC Day model. These models are also presented in Fig. 9. At an altitude of 3048 m, C_n^2 values between $2.5*10^{-17}$ and $5.3*10^{-17}$ $m^{-2/3}$ were calculated using the streamwise jitter rms approach. At this altitude, these experimentally extracted C_n^2 values strongly agree with the turbulence models. At an altitude of 1829 m, C_n^2 values between $5.0*10^{-17}$ and $2.5*10^{-16}$ $m^{-2/3}$ were calculated. Despite varying more, these calculated C_n^2 values still agree quite well with the turbulence models. The lowest altitude of 1524 m yielded C_n^2 values from $4.6*10^{-17}$ to $3.0*10^{-15}$ $m^{-2/3}$. As seen in Fig. 9, despite having a wide spread, the extracted C_n^2 values are still in agreement with literature. However, especially at lower altitudes, the figure would benefit from more data points. These C_n^2 approximated using the single axis jitter rms approach were also in agreement with previous atmospheric turbulence profiling experiments also conducted with AAOL-BC. See Refs. [22,23] for more details.

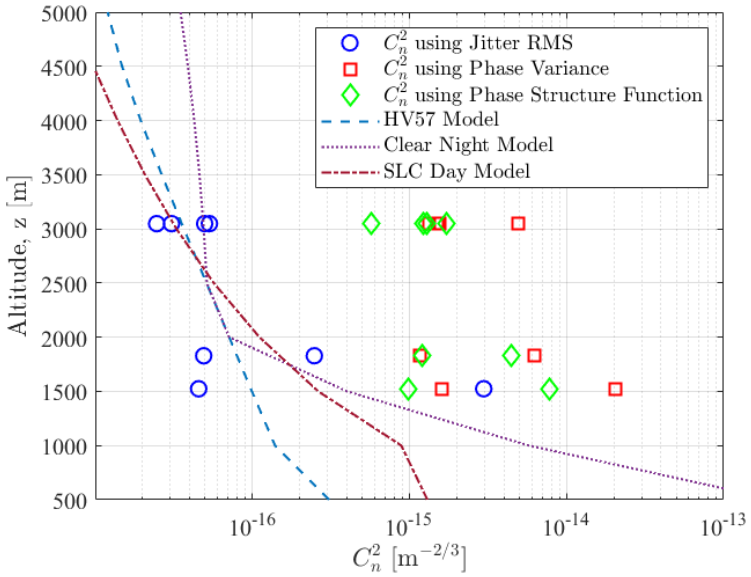

Figure 9. C_n^2 calculated from experimental data using three approaches. Conventional atmospheric turbulence models are also plotted for comparison.

In addition to comparing the extracted C_n^2 values with literature, the energy spectrum of the extracted jitter can also be compared with theory. According to literature, Eqs. 8 and 9 can be used to describe the theoretical low and high energy spectrum for Z-tilt, respectively [10]. These equations are slightly revised for environments of constant C_n^2. Here, D is the aperture diameter, f is the range of frequencies, L is the propagation distance, and U_∞ is the convective velocity.

$$\Phi(f)_{LOW} = 0.804 D^{-1/3} f^{-2/3} C_n^2 L (U_\infty)^{-1/3} \tag{8}$$

$$\Phi(f)_{HIGH} = 0.014 D^{-1/3} f^{-17/3} C_n^2 L (U_\infty)^{14/3} \tag{9}$$

For one of the data points above, a power spectrum is calculated on the experimentally stitched jitter time series. Using Eqs. 8 and 9, the empirical power spectrum will be compared with theory. The extracted C_n^2 value using the rms jitter approach is used as an input in these equations as well as the corresponding aperture size, propagation distance, and velocity for that data point. The results can be seen in Fig. 10. Here, the empirical Z-tilt energy spectrum is presented as a solid blue line, the theoretical low frequency spectrum is plotted as a dotted red line, and the theoretical high frequency spectrum is plotted as a dashed green line. It can be seen that specifically at high frequencies, the experimentally measured spectrum agrees well with theory. At low frequencies, the experimentally measured spectrum approaches the theoretical spectrum but is weaker than literature predicts. This is likely due to poor spectral convergence for large scale atmospheric turbulence structures. For future data collection, it may be beneficial to collect data at a lower sample rate but for lower time intervals.

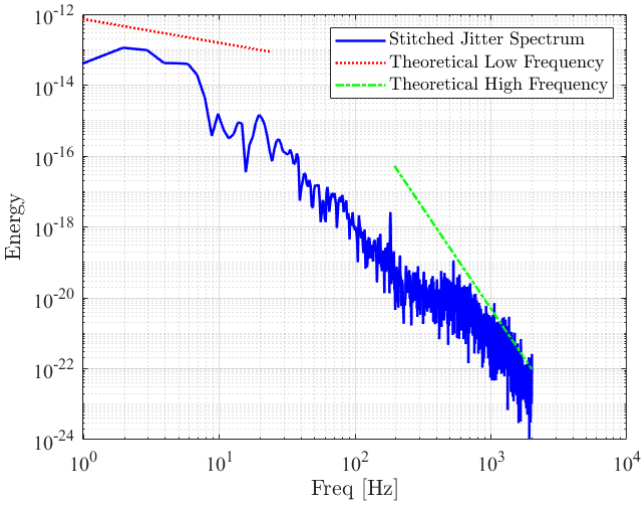

Figure 10. Experimentally measured tilt energy spectrum compared with theoretical low and high frequency Z-tilt energy spectrums.

VII. Conclusions

In this work, experiments were conducted which sought to quantify the atmospheric induced jitter on a laser beam at various propagation distances and altitudes. A data processing procedure for extracting the atmospheric induced tip/tilt is presented. It was shown that at low altitudes, up to 5 μrad of tilt was imposed onto the laser beam by the atmosphere. Using the atmospheric induced jitter, as well as higher order distortions, three methods of extracting optical turbulence parameters from the data were presented and compared with common altitude dependent atmospheric turbulence models. It was shown that for data points collected at all altitudes, the method which relied on the atmospheric induced jitter yielded C_n^2 calculations which closely matched the models prevalent in literature. The tilt removed phase variance approach and the phase structure function approach both overestimated the turbulence strength due to contamination from the aero-optical and aero-acoustical environment around the aircraft. An energy spectrum of the measured jitter was also calculated and compared with theory. It was shown that the experimentally measured tilt spectrum showed good agreement at high frequencies and some agreement at low frequencies.

VIII. Acknowledgments

This work is supported by the Joint Technology Office, Grant number FA9550-13-1-0001 and Office of Naval Research, Grant number N00014-18-1-2112. The U.S. Government is authorized to reproduce and distribute reprints for governmental purposes notwithstanding any copyright notation thereon.

References

[1] Andrews, L., and Phillips R., *Laser Beam Propagation Through Random Media*, SPIE-International Society for Optical Engineering, 2005.
[2] Tyler, G., "Bandwidth consideration for tracking through turbulence," Opt. Soc. Am., 11(1), 1994. 48
[3] Batchelor, G., *Homogeneous Turbulence*, Cambridge University Press, 1953.
[4] Kolmogorov, A.N., "The local structure of turbulence in incompressible viscous fluid for very large reynolds numbers," Dokl. Akad. Nauk SSSR, 30:301–305, 1940.
[5] Kolmogorov, A.N., "On degeneration of turbulence in incompressible viscous fluid," C.R. Akad. Sci. SSR (Dokl.), 31(6):538–541, 1941.
[6] Obukhov, A., "Temperature field structure in a turbulent flow," Izv. AN SSSR (Geogr. and Geophys. series), 13:58–69, 1949.
[7] Siegenthaler, J., Gordeyev, S., and Jumper, E.J., "Atmospheric propagation v. aerooptics," AIAA 2008-1076.
[8] Tatarskii, V., *Wave Propagation in a Turbulent Medium*, McGraw-Hill Book Company, 1961.
[9] Fried, D., "Optical heterodyne detection of an atmospherically distorted signal wave front," Proceedings of IEEE, 55(1), 1967.
[10] Tyson R., *Principles of Adaptive Optics*, Academic Press, 1998.
[11] Kalensky, M., Wells, J., Gordeyev, S., and Jumper, E.J., "Image degradation due to various aero-optical environments," In Proc. SPIE 11102, Applied Optical Metrology III. SPIE, 2019.
[12] Noll, R.J., "Zernike Polynomials and Atmospheric Turbulence," OSA, Vol. 66(3), pp. 207-211 (1976).
[13] Brennan, T.J., and Mann, D.C., "Estimation of Optical Turbulence Characteristics from Shack Hartmann Wavefront Sensor Measurements." Proc. SPIE, Vol. 7816, 781602-16, 2010.
[14] Kalensky, M., Gordeyev, S., and Jumper, E.J., "In-flight studies of aero-optical distortions around aaol-bc," In AIAA Aviation, 10.2514/6.2019-3253.
[15] Siegenthaler, J., *Guidelines for Adaptive Optic Correction Based on Aperture Filtration*, PhD dissertation, University of Notre Dame, 2008.
[16] Kemnetz, M., *Analysis of the Aero-Optical Component of Jitter Using the Stitching Method*, PhD dissertation, University of Notre Dame, 2019.
[17] Gordeyev, S., and Kalensky, M., "Effects of engine acoustics on aero-optical environment in subsonic flight," AIAA Journal, 10.2514/1.J059484,2020.
[18] Kalensky, M., Jumper, E. J., Gordeyev, S., "Preliminary Investigation of Jitter Induced by the Atmosphere on Laser Beam Propagation from an Airborne Platform," AIAA Aviation Virtual, June 15-19, 10.2514/6.2020-2819.
[19] Martin, J., and Flatté, S., "Intensity images and statistics from numerical simulation of wave propagation in 3-d random media," J. Opt. Soc. Am., 27(11), 1988.
[20] Martin, J., and Flatté, S., "Simulation of point-source scintillation through three-dimensional random media," J. Opt. Soc. Am., 7(5), 1990.
[21] Kalensky, M., Wells, J., Gordeyev, S., "Image degradation due to different in-flight aero-optical environments," Optical Engineering, DOI: 10.1117/1.OE.59.10.104104, 2020.
[22] Kalensky, M., Diskin, Y., Whiteley, M.R., et. al., "Turbulence Profiling Using AAOL-BC," AIAA Sci-Tech, 10.2514/6.2020-0682.
[23] Diskin, Y., Whiteley, M.R., Kalensky, M., et. al., "Atmospheric and Aero-Disturbance Characterization for DE System Applications," AIAA Aviation, 10.2514/6.2020-3234.